V European Conference on Computational Fluid Dynamics
ECCOMAS CFD 2010
J. C. F. Pereira and A. Sequeira (Eds)
Lisbon, Portugal, 14–17 June 2010

# BUOYANCY EFFECTS ON FORCED CONVECTION FROM A HORIZONTAL CYLINDER IN PARALLEL AND CONTRA FLOW

**Armando A. Soares**[*,†], **M. Duarte Naia**[*,††], **Norberto J. Gonçalves**[*,†††], **Abel Rouboa**[*,†]

[*]ECT-UTAD, Universidade de Trás-os-Montes e Alto Douro
Apartado 1013, 5001-801 Vila Real, Portugal
e-mail: asoares@utad.pt

[†]CITAB/UTAD, Quinta de Prados, Apartado 1013, 5001-801, Vila Real, Portugal
[††]CEMUC®, Dep. Eng. Mecânica - Pinhal de Marrocos, 3030-788 Coimbra, Portugal
[†††]GCEP, Centro de Física da Universidade do Minho, 4710-057 Braga, Portugal
e-mail: {duarte, njg, rouboa}@utad.pt

**Key words:** Finite difference, Mixed convection, Nusselt number, Richardson number, Cylinder

**Abstract.** *The purpose of this investigation is to study the mixed convection heat transfer from a horizontal cylinder, for both situations, when the imposed flow is oriented parallel (parallel flow regime) and in the opposing (contra flow regime) direction of gravity. The continuity, momentum, and energy equations are expressed in the stream function/vorticity formulation and solved using a second-order accurate finite difference method to determine the local and surface-averaged Nusselt numbers, the drag coefficient and to map the flow domain in terms of the temperature and flow fields near the cylinder. Two different thermal boundary conditions were considered at the cylinder surface: constant temperature (CT) and constant heat flux (CHF). Extensive numerical results elucidating the dependence of the flow and heat transfer characteristics on the Richardson number ($0 \leq Ri \leq 2$), Prandtl number ($1 \leq Pr \leq 100$) and Reynolds number ($5 \leq Re \leq 40$) are presented. Over this range of conditions, the flow is assumed to be steady. On the whole, for parallel flow regime, an increase in the Richardson number led to a raise in both Nusselt number and drag coefficient, for both CT and CHF boundary conditions. However, for contra flow regime, these trends were reversed. For both parallel flow and contra flow regimes, the aforementioned behaviours were more pronounced for CT boundary condition than that for the CHF boundary condition.*

## 1 INTRODUCTION

The problem of mixed convection heat transfer from a horizontal cylinder has received considerable attention in view of its practical application in heat exchangers, modern electronic equipment cooling and solar extraction systems.

In most practical situations free convection, how so ever small, is always present and thus heat transfer occurs in the mixed convection regime. In a given situation, the importance of mixed convection is gauged by the value of the so-called Richardson number (*Ri*) which is defined as the ratio of the Grashof number to the square of the Reynolds number ($Ri = Gr/Re^2$) and provides a measure of the influence of free convection in comparison with forced convection. Thus, a small value of the Richardson number ($Ri \to 0$), indicates that heat transfer occurs primarily by forced convection, conversely a big value of the Richardson number ($Ri \to \infty$) indicates that heat transfer occurs primarily by free convection. The mixed convection is believed to occur in between these two limits, *i.e.*, for $Ri \sim O(1)$ which corresponds to the case when the imposed velocity and that induced by buoyancy are of comparable magnitudes. Further complications arise depending upon the orientation of the cylinder with respect to the direction of flow. Thus, for instance, when the imposed flow is upward over a heated cylinder, the rate of heat transfer is enhanced due to the aiding buoyancy, whereas the rate of heat transfer will deteriorate in case of the downward flow over a heated cylinder (opposing flow). Similarly, there are situations when the buoyancy induced velocity is oriented normal to the imposed flow, thereby resulting in the so-called cross-flow configuration. Obviously, the cross-flow configuration shows a greater degree of asymmetry in velocity field than that in aiding or opposing buoyancy case. This work is, however, concerned with the aiding and opposing configurations. Nevertheless, a terse review of the previous literature is instructive prior to the presentation of the present study.

Among others, the influence of buoyancy on convective heat transfer in cross-flow at low Reynolds ($Re < 0.4$) was investigated experimentally by Collis and Williams [1], who derived a rough criterion for the onset of buoyancy effects as $Re = 1.85\,Gr^{0.35}$. The influence of free stream direction on the rate of heat transfer from a horizontal cylinder was investigated experimentally by Hatton *et al.* [2] who studied the problem for the range $10^{-2} < Re_D < 45$ and Rayleigh number $10^{-3} < Ra_D < 10$. An experimental correlation based on vectorial summation of forced and free convection was deduced. This approach is difficult to justify on physical grounds because Nusselt numbers are not vectors. Fand and Keswani [3] studied the rate of heat transfer in the combined free and forced convection from a horizontal cylinder to cross-flow of water flowing in upward, downward and horizontal directions. Bard [4, 5] solved numerically the problem of combined heat transfer from an isothermal cylinder with its axis horizontal and perpendicular to the free stream direction and with free stream parallel and opposite to the buoyancy flow for $1 < Re < 40$ and $0 < Gr < 5\,Re^2$ keeping Prandtl number at constant value of 0.7. Subsequently, Badr [6] also studied the effect of flow direction from aiding flow to opposing flow for air. Chang and Sa [7] examined numerically the effects of mixed, free and forced convection heat transfer on vortex shedding in the near wake of a heated/cooled circular cylinder, and their findings are consistent with the experimental results of Noto *et al.* [8] and the subsequent numerical study of Hatanaka and Kawahara [9]. Subsequently, Ahmad and Qureshi [10] solved, for a single value of the Prandtl number ($Pr = 0.7$) for air, the laminar mixed convection from a uniform heat flux horizontal cylinder in a cross-flow by using finite difference method for $1 \le Re_D \le 60$ and $0 \le Gr_D^* \le 1.6 \times 10^4$. The influence of buoyancy on heat transfer, wake

structure, temporal lift, and drag forces over heated/cooled cylinders at low Reynolds numbers ($Re = 2$, 40) has been investigated numerically by Patnaik *et al.* [11] for a circular cylinder placed in a vertical stream. Kieft *et al*. [12] have studied the effect of mixed convection from a heated cylinder in horizontal cross flow configuration and found that this configuration leads to asymmetrical flow patterns. The effects of mixed convection on the wake instability of a heated cylinder in contra flow have been investigated experimentally [13] and numerically [14]. More recently, Soares *et al.* [15] have studied the mixed convection from a cylinder to power-law fluids when the imposed velocity is normal to the direction of the velocity induced by the buoyancy. Depending upon the values of the Richardson number ($Ri$), Prandtl number ($Pr$), Reynolds number ($Re$), and the power-law index ($n$), they reported the contribution of free convection to be of the order of 10-15%. Subsequently, this work has been extended by Srinivas *et al.* [16] to stud the effects of aiding buoyancy on heat transfer from a cylinder in power-law fluids. Aside from the aforementioned studies based on the application of the complete field equations, some results have also been obtained by employing the standard boundary layer flow approximation, *e.g.* [17]. Furthermore, an examination of these survey articles shows that buoyancy forces enhance the heat transfer rate when they aid the forced flow and decrease the same when they oppose it. It is thus abundantly clear that, over the years, mixed convection from a heated circular cylinder has attracted a fair bit of attention from the experimental, analytical and numerical standpoints, *e.g.* see [18, 19], albeit most of these studies relate to air as the working fluid, *i.e.*, $Pr = 0.7$.

The aim of the present study is to obtain numerical solutions to the coupled Navier-Stokes and energy equations for laminar mixed convection around a horizontal circular cylinder for both situations; when the imposed flow is oriented parallel and in the opposing direction of gravity. Two different thermal boundary conditions were considered at the cylinder surface: constant temperature (CT) and constant heat flux (CHF). In particular, the governing equations have been solved numerically for the following ranges of conditions: Reynolds number ($5 \le Re \le 40$), Prandtl number ($1 \le Pr \le 100$) and Richardson number ($0 \le Ri \le 2$).

## 2 MATHEMATICAL FORMULATION

Consider the steady and incompressible flow of a Newtonian fluid normal to a circular heated cylinder of radius $a$. The constant free-stream velocity and temperature are $U_\infty$ and $T_\infty$ , respectively. The unconfined flow condition is simulated here by enclosing the heated circular cylinder in a circular outer boundary (of radius $R_\infty$), as shown in figure 1. The radius of the outer boundary is taken to be sufficiently large (54.6 radii away from the cylinder surface), to minimize the boundary effects on the flow and heat transfer at the cylinder surface. The imposed flow is assumed to be oriented parallel (vertically upward) or in the opposing (vertically downward) direction of gravity. The effect of temperature variation on thermo-physical fluid properties (density $\rho$, specific heat at constant pressure $c_p$, and thermal conductivity $k$) is considered negligible except for the body force term in the momentum equation (Boussinesq approximation) and the viscous dissipation term in the thermal energy equation neglected. The buoyancy force arises from the variation of the fluid density with temperature in the vicinity of the cylinder.

It needs to be emphasized here that the viscous dissipation term has been neglected in the energy equation used here because, for the range of conditions of $5 \le Re \le 40$, the shear rate close to the surface cylinder is not expected to be excessively high.

Since the present study is restricted to an infinite length of the cylinder axis along the $z$-direction and flow conditions of $Re \le 40$, the flow across the cylinder is steady and two dimensional. Thus, no flow variable depends upon the $z$ coordinate and thus $v_z = 0$. The relevant governing equations (continuity, momentum, and thermal energy) can be expressed in their dimensionless form in terms of the polar coordinates ($\varepsilon$, $\theta$) with $\varepsilon = \ln(r/a)$, see *e.g.*[15], giving:

$$\frac{1}{e^{\varepsilon}}\frac{\partial}{\partial \varepsilon}\left(e^{\varepsilon}\frac{\partial \psi}{\partial \theta}\right)-\frac{\partial}{\partial \theta}\left(\psi+\frac{\partial \psi}{\partial \varepsilon}\right)=0 \tag{1}$$

$\varepsilon$-component of momentum equation

$$\frac{\partial \psi}{\partial \theta}\frac{\partial^2 \psi}{\partial \varepsilon \partial \theta}-\left(\frac{\partial \psi}{\partial \varepsilon}+\psi\right)\left(\frac{\partial^2 \psi}{\partial \theta^2}+\frac{\partial \psi}{\partial \varepsilon}+\psi\right)=-\frac{1}{2}\frac{\partial p}{\partial \varepsilon}+\frac{Gr}{2Re^2}T\sin\theta -\frac{2^n}{Re}\left[e^{-\varepsilon}\frac{\partial}{\partial \varepsilon}\left(e^{\varepsilon}\tau_{rr}\right)+\frac{\partial \tau_{r\theta}}{\partial \varepsilon}-\tau_{\theta\theta}\right] \tag{2a}$$

$\theta$-component of momentum equation

$$-\frac{\partial \psi}{\partial \theta}\left(\frac{\partial^2 \psi}{\partial \varepsilon^2}+\frac{\partial \psi}{\partial \varepsilon}\right)+\left(\frac{\partial \psi}{\partial \varepsilon}+\psi\right)\frac{\partial^2 \psi}{\partial \varepsilon \partial \theta}=-\frac{1}{2}\frac{\partial p}{\partial \theta}+\frac{Gr}{2Re^2}T\cos\theta -\frac{2^n}{Re}\left[e^{-2\varepsilon}\frac{\partial}{\partial \varepsilon}\left(e^{2\varepsilon}\tau_{r\theta}\right)+\frac{\partial \tau_{\theta\theta}}{\partial \theta}\right] \tag{2b}$$

energy equation

$$\frac{\partial^2 T}{\partial \varepsilon^2}+\frac{\partial^2 T}{\partial \theta^2}-\frac{\partial T}{\partial \varepsilon}\left(2+\frac{e^{\varepsilon}RePr}{2}\frac{\partial \psi}{\partial \theta}\right)+\frac{\partial T}{\partial \theta}\left(\frac{e^{\varepsilon}RePr}{2}\left(\psi+\frac{\partial \psi}{\partial \varepsilon}\right)\right) +T\left(1+\frac{e^{\varepsilon}RePr}{2}\frac{\partial \psi}{\partial \theta}\right)=0 \tag{3}$$

where the dimensionless stream function $\psi$, vorticity $\omega$ and pressure $p$ are related to their dimensional counterparts as $e^{\varepsilon}U_{\infty}a\psi$, $e^{-\varepsilon}(U_{\infty}/a)\omega$ and $\left(U_{\infty}{}^2\rho/2\right)p$, respectively. The dimensionless components of the stress tensor $\tau_{ij}$ are related to their dimensional counterparts as $\eta(U_{\infty}/a)\tau_{ij}$. In the energy equation (eq.3), the dimensionless temperature is scaled in two different ways depending on the thermal boundary condition imposed at the cylinder surface ($\varepsilon = 0$). The two commonly used thermal boundary conditions at the cylinder surface are that of either a constant temperature ($T_s$) or a constant heat flux ($q_s$). Thus, for the constant temperature ($T_s$) boundary condition the dimensionless temperature $T$ is related to its dimensional counterparts as $e^{-\varepsilon}T(T_s - T_{\infty})$ whereas, for the constant heat flux boundary condition, the dimensionless temperature $T$ is related to its dimensional counterparts $e^{-\varepsilon}Tq_s a/k$.

The Reynolds number ($Re$) appearing in equations (2) and (3) is defined as

$$Re = \frac{\rho U_{\infty}(2a)}{\eta}, \tag{4}$$

where $\eta$ denotes the viscosity.
The Prandtl number is defined as

$$Pr = \frac{c_p \eta}{k}. \tag{5}$$

For the constant temperature boundary condition (CT), the Richardson number is defined as

$$Ri = \frac{Gr}{Re^2} = \frac{\beta g\left(T_s - T_{\infty}\right)(2a)}{U_{\infty}^2} \tag{6a}$$

and for the constant heat flux boundary condition (CHF) we use the modified Richardson number which is defined as

$$Ri^* = \frac{Gr^*}{Re^2} = \frac{\beta\, g\left(q_s a/k\right)(2a)}{U_{\infty}^2}, \tag{6b}$$

where $g$ is the gravitational acceleration and $\beta$ is the coefficient of volumetric expansion.

The dimensionless components of the stress tensor are written as

$$\tau_{ij} = -\eta\, \varepsilon_{ij}, \tag{7}$$

where $\eta$ is the dimensionless viscosity and $\varepsilon_{ij}$ are the dimensionless components of the rate-of-deformation tensor.

The vorticity in its scaled form is given as

$$\frac{\partial^2 \psi}{\partial \varepsilon^2} + \frac{\partial^2 \psi}{\partial \theta^2} + 2\frac{\partial \psi}{\partial \varepsilon} + \psi + \omega = 0. \tag{8}$$

Eliminating the pressure in equations (2) by the method of cross-differentiation, introducing the vorticity $\omega$ and doing some rearrangement, equation (8) can be expressed in the form

$$\eta\left(\frac{\partial^2 \omega}{\partial \varepsilon^2} + \frac{\partial^2 \omega}{\partial \theta^2}\right) + 2\lambda\frac{\partial \omega}{\partial \varepsilon} + 2\mu\frac{\partial \omega}{\partial \theta} + \gamma\,\omega = M, \tag{9a}$$

where

$$\lambda = \frac{\partial \eta}{\partial \varepsilon} - \eta - \frac{Re\quad e^{\varepsilon}}{4}\frac{\partial \psi}{\partial \theta}, \tag{9b}$$

$$\mu = \frac{\partial \eta}{\partial \theta} + \frac{Re\quad e^{\varepsilon}}{4}\left(\frac{\partial \psi}{\partial \varepsilon} + \psi\right), \tag{9c}$$

$$\gamma = -2\quad \frac{\partial \eta}{\partial \varepsilon} + \eta + \frac{Re\quad e^{\varepsilon}}{2}\frac{\partial \psi}{\partial \theta} \tag{9d}$$

and

$$M = \frac{Re\,Ri}{4} e^{\varepsilon} \left[ \frac{\partial T}{\partial \theta} \sin\theta - \left( \frac{\partial T}{\partial \varepsilon} - T \right) \cos\theta \right]. \tag{9e}$$

Owing the symmetry of the flow, the solution is obtained in the region defined by $0 \le \varepsilon \le \varepsilon_\infty$ and $\pi/2 \le \theta \le 3\pi/2$, see figure 1.

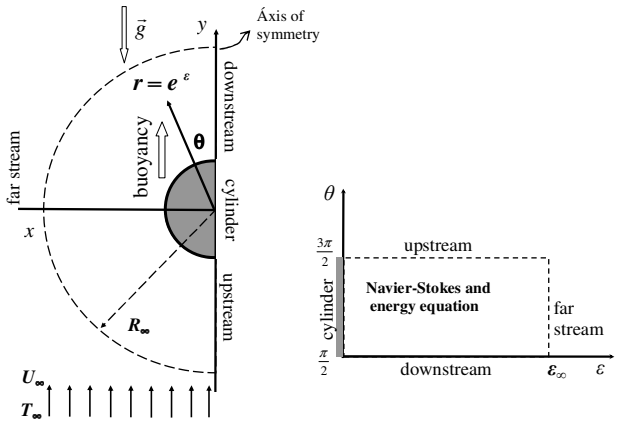


Figure 1: Real $(x, y)$ and computational $(\varepsilon, \theta)$ plane. Variables include gravitational acceleration ($g$), the free stream fluid temperature ($T_\infty$), and uniform approach velocity ($U_\infty$) when the imposed flow is upward over a heated cylinder.

The physically realistic boundary conditions for this flow problem are expressed as follows:

a) On the cylinder surface, *i. e.*, at $\varepsilon = 0$, the standard usual *no-slip* condition is applied. Thus

$$\frac{\partial \psi}{\partial \varepsilon} = \frac{\partial \psi}{\partial \theta} = 0, \tag{10a}$$

which together with eq. (8) gives

$$\psi = 0 \quad \text{and} \quad \omega = -\frac{\partial^2 \psi}{\partial \varepsilon^2}. \tag{10b}$$

The two commonly used thermal boundary conditions at the surface of the solid cylinder are scaled as

$$T = 1 \tag{10c}$$

for the constant temperature condition (CT) and

$$\frac{\partial T}{\partial \varepsilon} = T - 1 \tag{10d}$$

for the constant heat flux condition (CHF). The dimensionless temperature ($T$) used in the present study is related to the previously used (*e.g.* [15, 20]) dimensionless temperature in real space ($\overline{T}$) as $T = e^{\varepsilon}\overline{T}$.

b) On the plane of symmetry at $\theta = \pi/2, 3\pi/2$: the symmetry condition is imposed. Accordingly we put

$$\psi = \omega = \frac{\partial T}{\partial \theta} = 0. \tag{10e}$$

c) Far away from the cylinder surface, for $\varepsilon_\infty = 4$: we assumed the asymptotic approximation for stream function and vorticity given by Imai [21],

$$\psi \approx \sin(\theta - \alpha) + \frac{Cd}{2} e^{-\varepsilon} \left( \frac{\theta - \alpha}{\pi} - \text{erf}(Q) \right) \tag{10f}$$

and

$$\omega \approx -\frac{Cd\ Re}{4\sqrt{\pi}} Q\ e^{-Q^2}, \tag{10g}$$

where *Cd* is the drag coefficient,

$$Q = e^{\frac{\varepsilon}{2}} \sqrt{\frac{Re}{2}} \sin\left( \frac{\theta - \alpha}{2} \right) \tag{10h}$$

and erf(*Q*) is the standard error function. The parameter alpha is fixed as $\alpha = \pi/2$ and $3\pi/2$ for the contra flow and parallel flow regimes, respectively.

Finally the thermal boundary condition at $r = r_\infty$ is fixed as

$T = 0$ for CT and CHF conditions. (10i)

The numerical solution of the system of coupled elliptic governing equations, given by equations (3), (8) and (9) together with the above-noted boundary conditions provide the theoretical framework for mapping the flow domain, $0 \le \varepsilon \le 4$, in terms of the values of $\omega$, $\psi$ and *T*, which in turn can be processed further to obtain the values of the integral quantities, *i.e.,* the drag coefficient (*Cd*) and the local and surface-averaged Nusselt number (*Nu*) for the two thermal boundary conditions.
The total drag coefficient, given by

$$C_d = \frac{4}{Re} \int_{\pi/2}^{3\pi/2} \left( \frac{\partial \bar{\omega}}{\partial \varepsilon} - \bar{\omega} \right)_{\varepsilon=0} \sin\theta\ d\theta \tag{11}$$

where $\bar{\omega}$ is the dimensionless vorticity in real space ($\bar{\omega} = e^{-\varepsilon} \omega$).

The surface-averaged Nusselt number is given by

$$Nu = \frac{1}{\pi} \int_{\pi/2}^{3\pi/2} Nu(\theta)\, d\theta, \tag{12}$$

where $Nu(\theta)$ is the local Nusselt number on the cylinder surface. That function is given as (see [15])

$$Nu(\theta) = -2 \left( \frac{\partial T}{\partial \varepsilon} - T \right)_{\varepsilon=0}, \tag{13}$$

for the constant temperature boundary condition (CT), and as

$$Nu(\theta) = \left. \frac{2}{T} \right|_{\varepsilon=0}, \tag{14}$$

for the constant heat flux boundary condition (CHF).

Thus, in summary, once the values of the stream function, vorticity and temperature fields are known, these can be post-processed to obtain the values of drag coefficient, local and surface-averaged Nusselt numbers as functions of the kinematic variables (*Re*, *Ri*, *Pr*). These results elucidate the interplay between the kinematic variables and the flow when the imposed flow is oriented parallel and in the opposing direction of gravity.

## 3 NUMERICAL SOLUTION PROCEDURE

The numerical solutions were obtained for the computational domain shown in figure 1. For a $(N+1)\times(M+1)$ computational mesh, the spacing in the $\varepsilon$ and $\theta$ directions are $\varepsilon_\infty/N$ and $\pi/M$, respectively. The set of governing stream function, vorticity and energy equations (8) and (9) which are coupled by the buoyant term (eq.9e) have been solved by a finite difference scheme using a second order upwind differencing technique to discretize the convective terms of $T$ and $\omega$ in the vorticity and energy equations, whereas for the diffusion terms, the central difference approximation was used. For all other terms in these equations, central difference approximations have also been employed. The resulting system of equations was solved using a Gauss-Seidel iterative method with an under relaxation factor between 0.5 and 1 to the temperature and vorticity variables. For each of the two thermal surface boundary conditions, to obtain consistent approximations for all variables, for each iteration a sweep is made through all mesh points and an updated value of the drag coefficient and of the Nusselt number *Nu*, are determined by numerical integration of eqs. (11) and (12) on the cylinder surface using Simpson's rule. The values of $\psi$, $\omega$ and $T$ obtained at every point for the pure forced convection ($Ri = 0$) solutions, were used as the initial guesses for the mixed convection ($Ri \neq 0$). This procedure ensured accelerated convergence of the numerical solution. Convergence was achieved when the variation in the both values of the drag coefficient and Nusselt number in two successive iterations was less than a preset value of $10^{-8}$. In general, it is somewhat easier to meet the convergence criterion for constant heat flux boundary condition (CHF) than that for constant temperature boundary condition (CT), although in both cases, for $Ri \neq 0$, the difficulty to meet the convergence criterion increases as the value of *Pr* decreases. The outer boundary was positioned at $\varepsilon_\infty = 4$, corresponding to asymptotic boundary conditions at a distance of ~54.6 radii away from the cylinder. For all range of conditions, a mesh with 201×101 points were used in radial and angular directions, respectively. Additional tests carried out for the largest values of the Reynolds, Prandtl and Richardson numbers showed that the grid was adequate to obtain sufficient numerical resolution.

## 4 RESULTS AND DISCUSSION

The governing differential equations of flow and heat transfer for the mixed convection regime have been solved numerically to investigate the effects of Richardson numbers ($Ri$ and $Ri^* = 0, 0.5, 1, 2$), Reynolds number ($5 \le Re \le 40$) and Prandtl ($0 \le Pr \le 100$) number on the flow and heat transfer characteristics for the two thermal boundary conditions on the cylinder surface (CT and CHF boundary conditions). Extensive results on the streamline patterns, surface vorticity, drag coefficient (*Cd*), isotherm patterns, and local ($Nu(\theta)$) and surface-averaged (*Nu*) Nusselt numbers have been obtained to elucidate the influence of buoyancy effects on the rate of heat transfer from a circular cylinder to Newtonian fluids, when the imposed flow is oriented parallel and in the opposing direction of gravity.

For the Prandtl number values used in this work the contribution of free convection can be assessed over the whole range of Prandtl numbers (*Pr*). The 100-fold variation in the value of *Pr* covered in this work should provide an adequate guide for delineating the scaling of the Nusselt number (*Nu*) with Prandtl number. It is appropriate to add here that it is not at all uncommon to encounter industrial fluids possessing the value of Prandtl number as large as 100, or even higher. Besides, in numerical studies, the maximum value of the *Pr* is also restricted by the fact that very fine grids are required near the cylinder owing to the progressive thinning of the thermal boundary layer with increasing Prandtl number.

The Richardson number values are chosen as *Ri* and $Ri^* = 0, 0.5, 1, 2$ , so that $Ri = 0$ case corresponds to forced convection, whereas at $Ri = 1$ the characteristics velocity induced by density variation is of the same order as the imposed flow velocity. The case of $Ri = 2$ corresponds to the situation in which strong free convection effects are expected. At the outset it is, however, important to validate the numerical solution procedure, as this will help establish the accuracy of the new results presented in this study.

### 4.1. VALIDATION OF NUMERICAL SOLUTION PROCEDURE

The numerical solution procedure has been benchmarked using some of the results available in the literature.

For both parallel flow and contra flow regimes, the surface-averaged Nusselt number (*Nu*) of the present results using the constant temperature boundary condition (CT) are compared, in table 1, with the numerical predictions of Badr [5], for $Re = 5$, 20 and 40 when $Pr = 0.7$, whereas table 2 shows the comparison between the present numerical results of Nusselt (*Nu*) and coefficient drag (*Cd*) with those obtained by Srivinas *et al.* [16] for $Re = 5$, and 40 in the range $1 \le Pr \le 100$.

For the parallel flow, an excellent correspondence can be seen to exist between the present results of the surface-averaged Nusselt number (*Nu*) and those of reference for $Re = 5$, 20 and 40, and $0.7 \le Pr \le 100$ (see table 1 and 2). The maximum difference being of the order of ~7% and ~4% from those of Bard and Srinivas, respectively. Deviations of this order are not at all uncommon in such numerical studies and these arise due to differences in the numerical methods (for instance finite volume method used by Srinivas et al. [16] versus finite difference method used here), problem formulations, flow schematics, grid and/or domain sizes, discretization schemes, etc.

On the other hand, the present results for the coefficient drag values were compared with the literature values, *e.g.* [16]. Under these conditions, as expected, our results always showed an increase of *Cd* with *Ri* consistent with published numerical results of Srinivas. For $Ri = 0$, the two values of the coefficient drag (*Cd*) are in excellent agreement (discrepancies 2.2% and 0.1% at $Re = 5$ and 40, respectively). However, for $Ri = 2$ and $Pr = 100$, the maximum discrepancies increased to 32% and 57% at $Re = 5$ and 40, respectively.

For contra flow, the present numerical results for the surface-averaged Nusselt number were compared with numerical predictions of Badr [5]. From table 1, it is clearly seen that, for $Re = 5$, 20 and 40, the present results deviate at most by 45%, 8%, and 29%, from those of Badr, respectively. Finally, attention is drawn to the fact that the present results for $Ri = 0$ are in excellent agreement with the literature values [22] where the discrepancy between the numerical results for $Ri = 0$ given by the different authors did not exceed 5%. On the other hand, the vorticity distribution around the cylinder surface at $Re = 20$ and 40 for different values of *Ri* in the parallel flow can be seen in figure 2. This figure can be compared with the Bard [5] figures under the same

conditions and an excellent agreement is found. For instance, an increase in *Ri* from 0 to 4 resulted, for *Re* = 20 and 40, in an increase in the maximum of surface vorticity magnitude from 4.03 to 11.77 and from 5.82 to 15.78, respectively. These observations are in excellent agreement with the figures 1(a) and (b) obtained by Bard in ref. [5]. The flow separation are only observed for *Ri* = 0 and 0.25. The comparison of the angles of separation between the present results and Bard´s (results) showed discrepancies of less than 1% for both *Re* = 20 and 40.

| | | *Nu* | | *Nu* | |
|---|---|---|---|---|---|
| | | *Parallel flow* | | *Contra flow* | |
| *Re* | *Ri* | present | Badr[5] | present | Badr[5] |
| 5 | 0 | 1.45 | 1.450 | 1.45 | - |
| | 0.2 | 1.53 | 1.499 | 1.29 | 2.37 |
| | 2.4 | 1.87 | 1.882 | - | - |
| | 4 | 2.00 | 1.995 | - | - |
| | 5 | 2.06 | 2.075 | - | - |
| 20 | 0 | 2.42 | 2.540 | 2.42 | - |
| | 0.5 | 2.61 | 2.654 | 2.00 | 2.12 |
| | 1 | 2.90 | 2.970 | 1.73 | 1.78 |
| | 2 | 3.12 | 3.227 | 2.32 | 2.15 |
| | 3 | 3.28 | 3.420 | - | - |
| | 4 | 3.41 | 3.564 | - | - |
| 40 | 0 | 3.19 | 3.480 | 3.19 | - |
| | 0.25 | 3.45 | 3.650 | 2.67 | 3.17 |
| | 0.5 | - | - | 2.25 | 3.05 |
| | 1 | 3.85 | 4.100 | 2.06 | 2.70 |
| | 2 | 4.16 | 4.420 | 4.16 | 3.22 |
| | 3 | 4.39 | 4.690 | - | - |
| | 4 | 4.57 | 4.910 | - | - |

Table 1: Comparison between the *Nu* results of Bard [5] and present predictions using the CT boundary condition for *Pr* = 0.7.

| | | present | | | | Srinivas et al.[16] | | | |
|---|---|---|---|---|---|---|---|---|---|
| | | *Re=5* | | *Re=40* | | *Re=5* | | *Re=40* | |
| *Pr* | *Ri* | *Cd* | *Nu* | *Cd* | *Nu* | *Cd* | *Nu* | *Cd* | *Nu* |
| 1 | 0 | 4.08 | 1.60 | 1.50 | 3.58 | 3.9365 | 1.5619 | 1.4987 | 3.6526 |
| | 1 | 9.90 | 1.88 | 4.30 | 4.31 | 8.9774 | 1.9115 | 2.9586 | 4.4812 |
| | 2 | 14.35 | 2.02 | 6.60 | 4.66 | 12.1298 | 2.0610 | 3.8225 | 4.8582 |
| 10 | 0 | 4.08 | 3.15 | 1.50 | 7.79 | 3.9365 | 3.1810 | 1.4987 | 8.0605 |
| | 1 | 7.89 | 3.56 | 3.83 | 8.82 | 6.5888 | 3.6773 | 2.3979 | 9.2160 |
| | 2 | 11.02 | 3.78 | 5.80 | 9.49 | 8.3508 | 3.9291 | 2.8996 | 9.9329 |
| 20 | 0 | 4.08 | 3.89 | 1.50 | 9.89 | 3.9365 | 3.9553 | 1.4987 | 10.2412 |
| | 1 | 7.47 | 4.34 | 3.72 | 10.95 | 6.0944 | 4.4960 | 2.2670 | 11.4214 |
| | 2 | 10.32 | 4.59 | 5.63 | 11.75 | 7.5637 | 4.7838 | 2.6926 | 12.2613 |
| 50 | 0 | 4.08 | 5.16 | 1.50 | 13.67 | 3.9365 | 5.2910 | 1.4987 | 14.0449 |
| | 1 | 7.02 | 5.67 | 3.60 | 14.66 | 5.5579 | 5.8887 | 2.1173 | 15.1594 |
| | 2 | 9.57 | 5.97 | 5.44 | 15.64 | 6.7028 | 6.2261 | 2.4579 | 16.1785 |
| 100 | 0 | 4.08 | 6.42 | 1.50 | 17.51 | 3.9365 | 6.6071 | 1.4987 | 17.9168 |
| | 1 | 6.75 | 6.97 | 3.53 | 18.23 | 5.2304 | 7.2463 | 2.0217 | 18.7893 |
| | 2 | 9.12 | 7.31 | 5.32 | 19.37 | 6.1710 | 7.6219 | 2.3079 | 19.9606 |

Table 2: Comparison between the *Nu* results of Srinivas *et al.*[16] and present predictions using the CT boundary condition, for parallel flow regime.

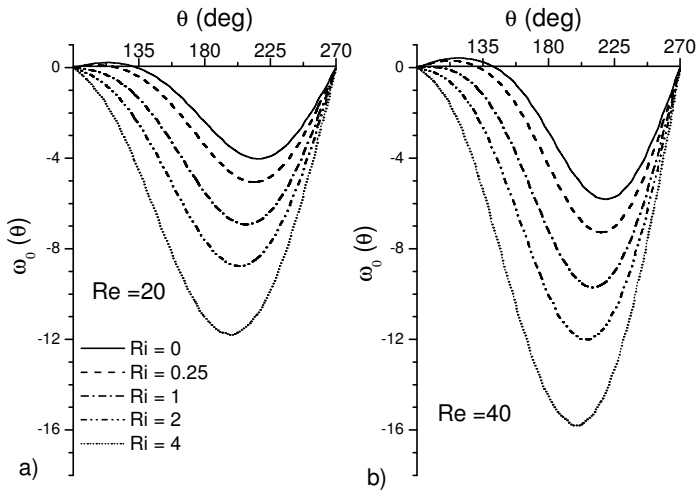


Figure 2: The vorticity distribution on the cylinder surface at different values of *Ri* for the case of parallel flow when *Pr* =0.7, using the CT boundary condition. a) *Re*= 20 and b) *Re* =40.

## 4.2. FLUID FLOW CHARACTERISTICS

Representative streamline patterns close to the cylinder for Reynolds numbers *Re* = 5 and 40, Richardson numbers *Ri* = 0, 0.5 and 2, Prandtl number *Pr* = 1, 10, 20, 50 and 100, in parallel flow and contra flow regimes are shown in figures 3 and 4, respectively. For constant temperature (CT) boundary condition (left half of the figures) and constant heat flux (CHF) boundary condition (right half of the figures).

For the parallel flow regime, figure 3, for both thermal boundary conditions on the cylinder showed that for a fixed value of the Reynolds number *Re* an increase in Richardson number and/or a decrease in Prandtl number resulted in a decrease in distance between the streamlines. This effect is seen to be more marked in the downstream region than that in the upstream region and for the constant temperature (CT) boundary condition than that for constant heat flux (CHF) boundary condition. On other hand, in the case of forced convection *Ri* = 0, due to the decoupling between the momentum and energy equations, the flow field is not influenced by Prandtl number. At low Reynolds number (*Re* = 5), no separation was observed for any value of the Richardson number in the range of conditions studied herein. For CT boundary condition (left half of the figures), at *Re* = 40, can be seen that the size of wake decreases with increasing Richardson numbers (*Ri*) and/or Prandtl number (*Pr*). These findings are consistent with those reported in the literature [6, 11, 16]. However, for CHF boundary condition (right half of the figures), an opposite trend is seen for the behaviour of the wake with Prandtl number (*Pr*).

For the contra flow regime, figure 4, for both thermal boundary conditions on the cylinder surface showed that for a fixed value of the Reynolds number (*Re*) an increase in Richardson number (*Ri*) and/or a decrease in Prandtl number (*Pr*) resulted in an increase in distance between the streamlines, and in an increase in wake. However, for a fixed value of *Ri*, as the value of the Prandtl number was progressively decreased there was a decreasing degree of convergence.

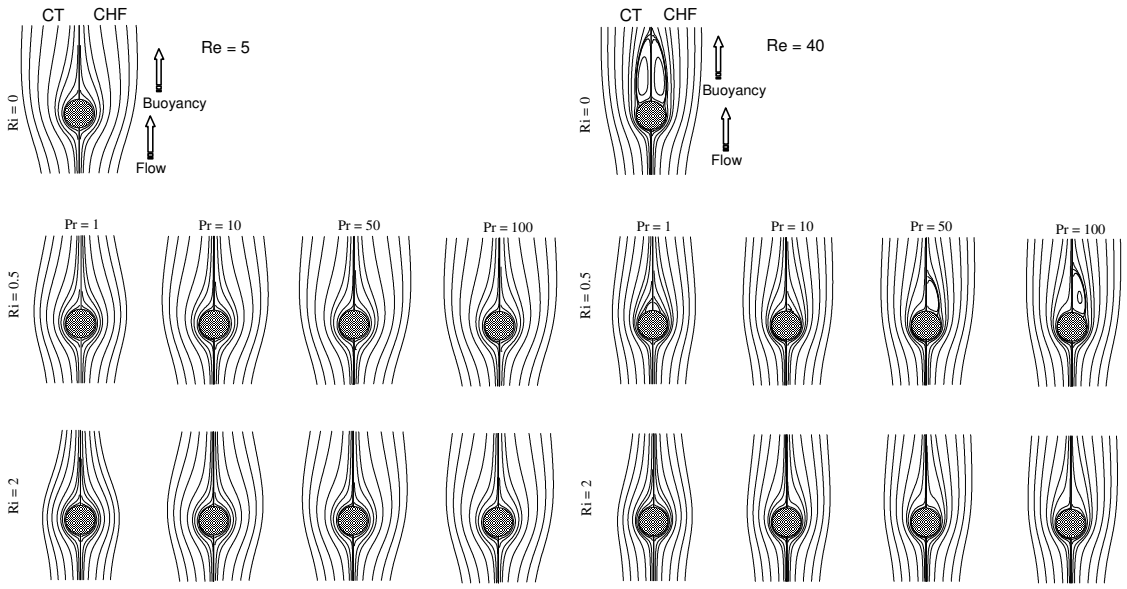


Figure 3: Influence of Richardson number (*Ri*) on the streamline for constant temperature (CT) boundary condition (left half of the figures) and constant heat flux (CHF) boundary condition (right half of the figures) at *Re* = 5 and 40 for *Pr* = 1, 10, 50 and 100. Parallel flow regime.

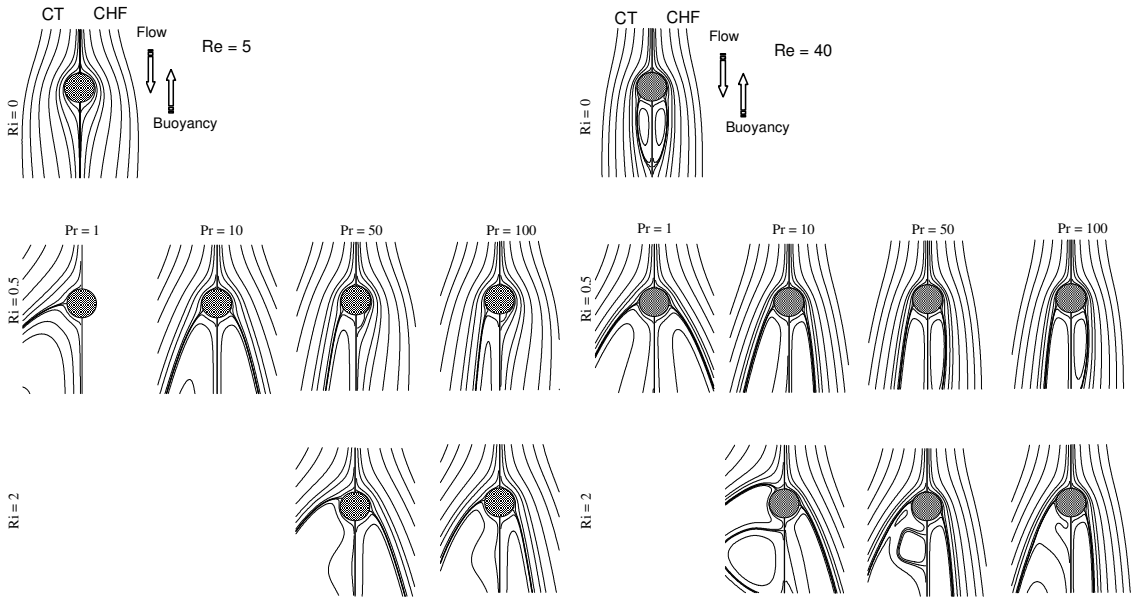


Figure 4: Influence of Richardson number (*Ri*) on the streamline for constant temperature (CT) boundary condition (left half of the figures) and constant heat flux (CHF) boundaryc ondition (right half of the figures) at *Re* = 5 and 40 for *Pr* = 1, 10, 50 and 100. Contra flow regime.

For the parallel flow regime, figure 5, the study of the vorticity contours around the cylinder surface showed that an increase in the Richardson number resulted in an overall increase of the vorticity magnitude, except for *Re* = 40 in the wake, where this trend was reversed. This trend is qualitatively similar to that observed by Badr [5] for *Pr* = 0.7. This trend is less pronounced for higher values of *Pr* and for CHF condition than that for CT condition. For instance, for CHF condition, an increase in *Ri* from 0 to 2 resulted, for *Pr* = 1, in an increase in maximum of the $|\omega_0(\theta)|$ of 125.4% at *Re* = 5 and 51.8% at *Re* = 40; the corresponding increases for *Pr* = 100 were 7.7% and 7.1%. For CT condition, under the same conditions, the corresponding increases for *Pr* = 1 were 137.6% and 97.3%, for *Pr* = 100 were 26.3% and 27.8%. Furthermore, the figure 5

showed that the separation angle were strongly dependent on the Richardson number and Prandtl number for $Re = 40$.

For the contra flow regime, figure 6, an opposite behaviour was observed for the surface vorticity to that observed for the parallel flow regime, whereas for lower Reynolds number ($Re = 5$), the increase of the $|\omega_0(\theta)|$ in the wake region with $Ri$ was much pronounced for CT condition.

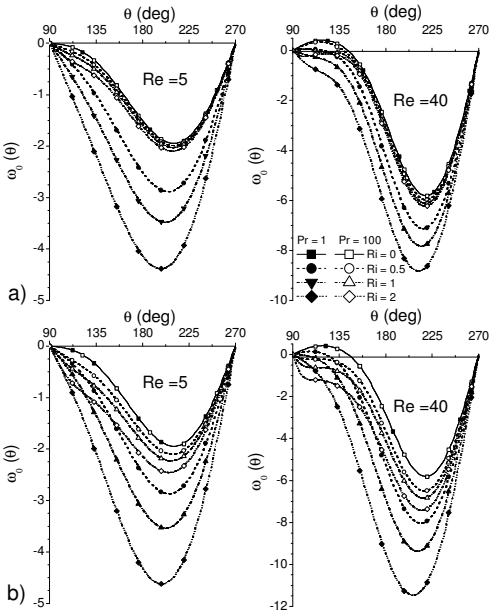


Figure 5: The vorticity distribution on the cylinder surface at different values of $Ri$ for the case of parallel flow when $Pr = 1$ and 100 at $Re = 5$ and 40 using the a) CHF boundary condition and b) CT boundary condition. (downstream $\theta = 90º$ and upstream $\theta = 270º$)

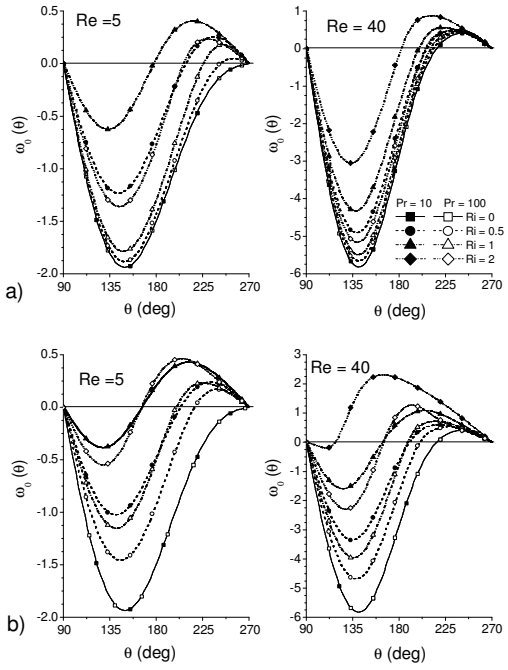


Figure 6: The vorticity distribution on the cylinder surface at different values of $Ri$ for the case of contra flow when $Pr = 10$ and 100 at $Re = 5$ and 40 using the a) CHF boundary condition and b) CT boundary condition. (downstream $\theta = 270º$ and upstream $\theta = 90º$)

The results for the normalized coefficient drag with respect to the corresponding pure forced convection *(Cd**), using both thermal boundary conditions(CT and CHF) is shown in figures 7 and 8, for the parallel flow and contra flow regimes, respectively. The results showed that, for parallel flow, an increase in the *Ri* caused an increase in the *Cd**, whereas an increase in the *Pr* caused a decrease in the *Cd**, for both boundary conditions. However, for the mixed convection ($Ri \neq 0$), figures 7a) and 7b) further show that, for CT condition, *Cd** was an increasing function of *Re*, whereas for CHF condition at $Pr = 1$, *Cd** was a decreasing function of *Re*, and at $Pr = 100$ became almost independent of the *Re*.

For the contra flow regime, Figure 8, an opposite behaviour was observed for the normalized coefficient drag (*Cd**). The results showed that, for contra flow, an increase in the *Ri* caused a decrease in the *Cd**, whereas an increase in the *Pr* caused an increase in the *Cd**, for both boundary conditions. Figures 8a) and 8b) further show that, for a fixed values of *Ri* and *Pr*, for CT condition *Cd** was a decreasing function of *Re*, whereas for CHF condition *Cd** was an increasing function of *Re*. Furthermore, the *Cd** decreases with *Ri* and becomes negative, due to reverse flow in the wake of the cylinder. Also, the dependence of the *Cd** on the *Ri* became more pronounced at higher Reynolds numbers for CT condition, whereas this trend was reversed for the CHF condition.

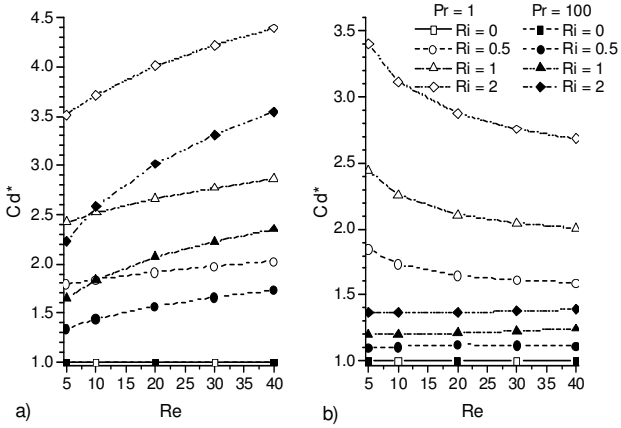


Figure 7: Variation of the normalized drag coefficient ($Cd^*$) with Reynolds number (*Re*) and Richardson number (*Ri*) for $Pr = 1$ and 100 in parallel flow regime. a) CT condition b) CHF condition.

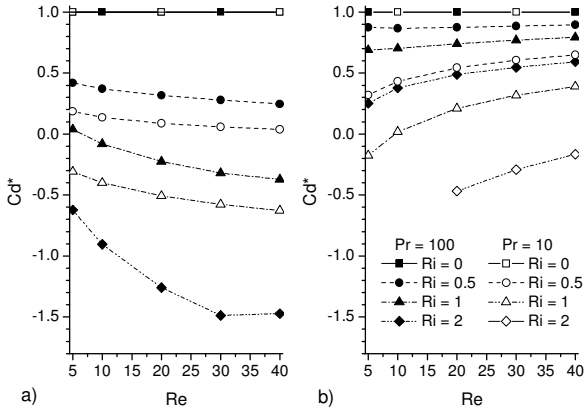


Figure 8: Variation of the normalized drag coefficient ($Cd^*$) with Reynolds number (*Re*) and Richardson number (*Ri*) for $Pr = 10$ and 100 in contra flow regime. a) CT condition b) CHF condition.

## 4.3. HEAT TRANSFER CHARACTERISTICS

Representative isotherm patterns close to the cylinder for Reynolds numbers $Re$ = 5 and 40, Richardson numbers $Ri$ = 0, 0.5, 1 and 2, Prandtl number $Pr$ = 1, 10, 20, 50 and 100, in parallel flow and contra flow regimes are shown in figures 9 and 10, respectively. For constant temperature (CT) boundary condition (right half of the figures) and constant heat flux (CHF) boundary condition (left half of the figures).

For the parallel flow regime, both thermal boundary conditions on the cylinder surface showed that, for a fixed value of the Reynolds number ($Re$), an increase in Richardson number ($Ri$) and/or Prandtl number ($Pr$) resulted in a decreasing distance between the isotherms, and the subsequent crowding of isotherms in the upstream direction. This behaviour means an increase temperature gradient, and, hence, the heat transfer rate increase with $Re$, $Pr$ and $Ri$. This effect is seen to be more marked for the constant temperature (CT) boundary condition than that for constant heat flux (CHF) boundary condition. These findings are consistent with those reported by Srinivas *et al.* [16] for the constant temperature (CT) boundary condition in Newtonian fluids.

For the contra flow regime, figure 10, both thermal boundary conditions on the cylinder surface showed that, for a fixed value of the Reynolds number $Re$, an increase in Richardson number ($Ri$) and/or a decrease in Prandtl number ($Pr$) resulted in a progressive detachment of the isotherms as well as in upstream convection of the isotherms. This behaviour can be explained in terms of the enhancement of the free convection contribution to the heat transfer due to the increase in the Richardson number ($Ri$) and the decrease in the Prandtl number ($Pr$), under the aforementioned conditions.

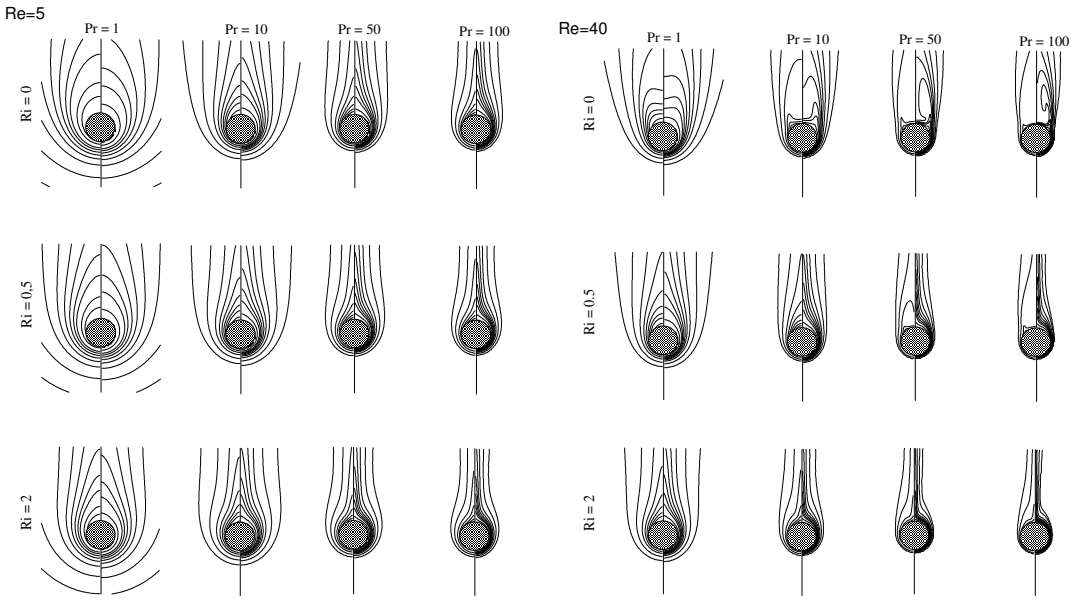


Figure 9: Influence of Richardson number ($Ri$) on the isotherms patterns for constant heat flux (CHF) boundary condition (left half of the figures) and constant temperature (CT) boundary condition (right half of the figures) at $Re$ = 5 and 40 for $Pr$ = 1, 10, 50 and 100. Parallel flow regime.

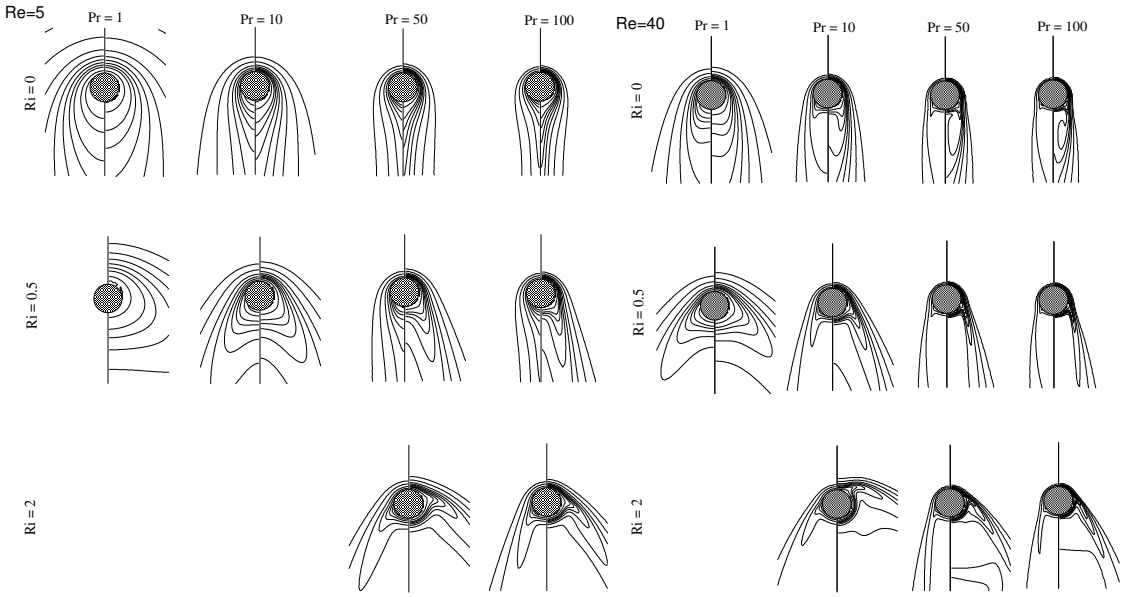


Figure 10: Influence of Richardson number (*Ri*) on the isotherms patterns for constant heat flux (CHF) boundary condition (left half of the figures) and constant temperature (CT) boundary condition (right half of the figures) at $Re = 5$ and 40 for $Pr = 1$, 10, 50 and 100. Contra flow regime.

For parallel flow regime, the study of the local Nusselt number $Nu(\theta)$ distribution on the cylinder surface showed that for $Pr = 1$ to 100, $Re = 5$, 40 and $Ri = 0$, 0.5, 1 and 2, for both thermal boundary conditions on the cylinder surface, local Nusselt number $Nu(\theta)$ was an increasing function of *Re, Pr* and/or *Ri*, except for $Re = 40$ at the rear of the cylinder ($\theta = 90º$) where the dependence of $Nu(\theta)$ on *Ri* is different (figure 11). At first, rear of the cylinder ($\theta = 90º$), a small increase in *Ri* causes a decrease in $Nu(\theta)$ until reaching its minimum value. A further increase in *Ri* results in increasing $Nu(\theta)$ rear of the cylinder. Thus, the results showed that an increase in the *Ri* caused an overall increase in the local Nusselt number. Also, for a fixed values of *Re* and *Pr*, the dependence of the $Nu(\theta)$ on the Richardson number (*Ri*) was more pronounced in downstream region and for CT boundary condition than that for CHF boundary condition (see figure 11).

For the contra flow regime, shown in figure 12, it was observed the opposite behaviour for the local Nusselt number. Thus, the results showed that an increase in the *Ri* caused an overall decrease in the local Nusselt number, except for the wake at the rear of the cylinder ($\theta = 270º$) where $Nu(\theta)$ increase with *Ri*. Furthermore, the dependence of the local Nusselt number on the Richardson number was more pronounced for the contra flow regime than that for parallel flow regime.

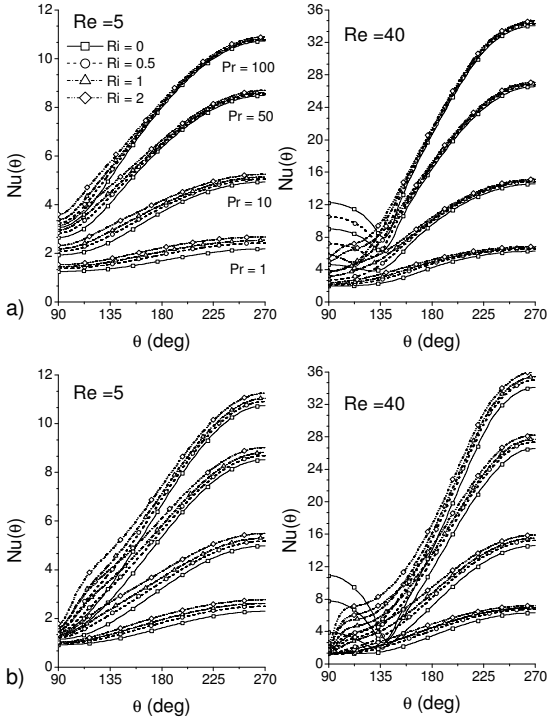


Figure 11: Local Nusselt number distribution on the cylinder surface at different values of *Ri* and *Pr* for the case of parallel flow at *Re* = 5 and 40 using the a) CHF condition and b) CT condition (downstream $\theta = 90°$ and upstream $\theta = 270°$).

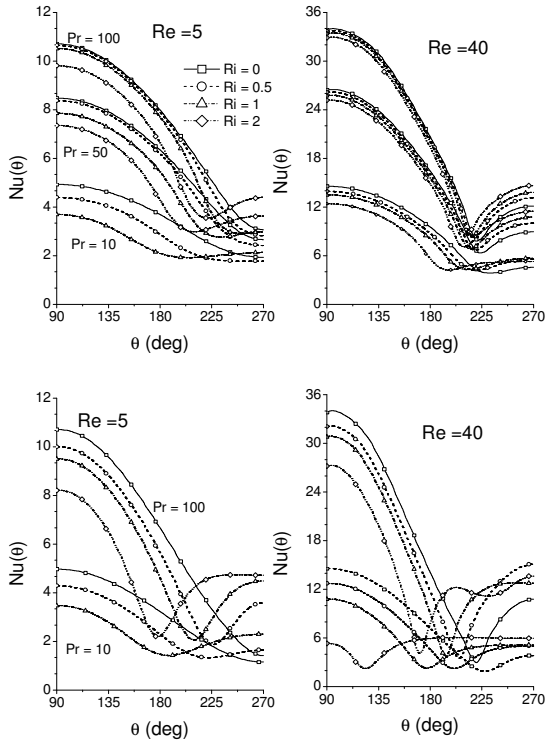


Figure 12: Local Nusselt number distribution on the cylinder surface at different values of *Ri* and *Pr* for the case of contra flow at *Re* = 5 and 40 using the a) CHF condition and b) CT condition. (downstream $\theta = 270°$ and upstream $\theta = 90°$).

The results for the normalized surface-averaged Nusselt number with respect to the corresponding pure forced convection (*Nu**), using both the constant temperature (CT) and constant heat flux boundary (CHF) conditions is shown in figures 13 and 14, for the parallel flow and contra flow regimes, respectively. The results showed that, for parallel flow, at $Pr = 1$ an increase in the *Ri* caused an increase in the *Nu**, whereas at $Pr = 100$ and $Re > 20$ this trend was only observed for $Ri \geq 1$ for both thermal boundary conditions.

For the contra flow regime, figure 14, the opposite behaviour was observed for the normalized surface-averaged Nusselt number (*Nu**). Hence, the results showed that an increase in the *Ri* implicated a decrease in the value of *Nu**, whereas at $Pr = 100$ and $Re > 20$ this trend was only observed for $Ri > 0.5$, for both thermal boundary conditions.

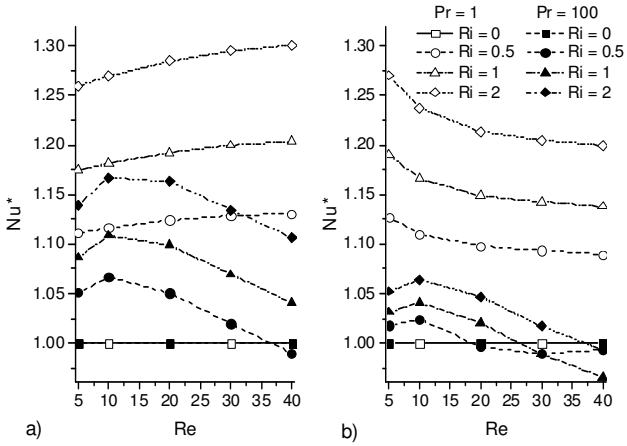


Figure 13: Variation of the normalized surface-averaged Nusselt number with Reynolds number and Richardson number for $Pr = 1$ and 100 in parallel flow regime. a) CT boundary condition, b) CHF boundary condition.

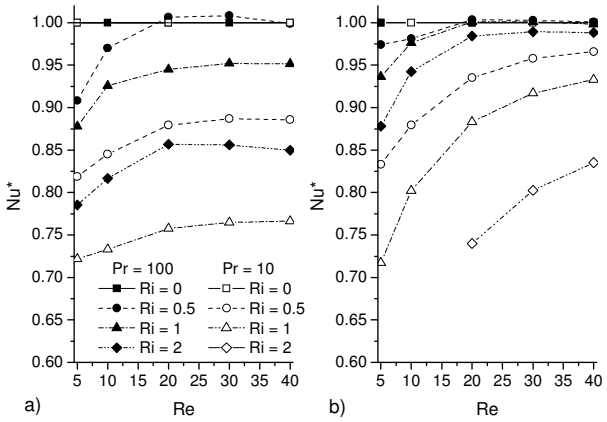


Figure 14: Variation of the normalized surface-averaged Nusselt number with Reynolds number and Richardson number for $Pr = 10$ and 100 in contra flow regime. a) CT boundary condition, b) CHF boundary condition.

## 5 CONCLUSIONS

The steady cross-flow over a heated circular cylinder, for the two cases of parallel and contra flow regimes, has been investigated numerically to determine the effect of the Richardson number on the flow and heat transfer characteristics in a wide range of Richardson number ($0 \leq Ri \leq 2$), Reynolds numbers ($5 \leq Re \leq 40$) and Prandtl

numbers ($1 \le Pr \le 100$). For parallel flow regime, streamline and isotherms patterns close to the cylinder showed that, for a fixed values of the *Re* and *Pr,* an increment in *Ri* resulted in an decrease in distance between the contour lines, for both streamlines and isotherms. The local Nusselt number and vorticity contours around the cylinder surface showed that an increase in the *Ri* resulted in an overall increase of the $Nu(\theta)$ and vorticity magnitude, respectively, except for in the wake, where this trend was reversed. Furthermore, an increase in the *Ri* led to the enhancement of *Cd** and *Nu**, for both CT and CHF boundary conditions. However, for contra flow regime all these trends were reversed. On the other hand, for both flow regimes the aforementioned behaviours was more pronounced in CT boundary condition case than in the CHF boundary condition.

## REFERENCES

[1] D.C. Collis, M.J. Williams, Two-dimensional convection from heated wires at low Reynolds number. *J. Fluid Mech*. **9**, pp. 357–384 (1959).

[2] A.P. Hatton, D.D. James, H.V. Swire, Combined forced and natural convection with low-speed air flow over horizontal cylinders. *J. Fluid Mech.* **42**, pp.17–31 (1970).

[3] R.M. Fand, K.K. Keswani, Combined natural and forced convection heat transfer from horizontal cylinders to water. *Int. J. Heat Mass Transfer* **16**, pp. 1175–1191 (1973).

[4] H.M. Badr, A theoretical study of laminar mixed convection from a horizontal cylinder in a cross stream. *Int. J. Heat Mass Transfer* **26**, pp. 639-653 (1983).

[5] H.M. Badr, Laminar combined convection from a horizontal cylinder parallel and contra flow regimes. *Int. J. Heat Mass Transfer* **27**, pp. 15-27 (1984).

[6] H.M. Badr, On the effect of flow direction on mixed convection from a horizontal cylinder. *Int. J. Numer. Meth. Fluids* **5**, pp. 1-12 (1985).

[7] K.-S Chang, J.-Y Sa, The effect of buoyancy on vortex shedding in the near wake of a circular cylinder. *J. Fluid Mech*. **220**, pp. 253-266 (1990).

[8] K. Noto, H. Ishida, R. Matsumoto, A breakdown of the Karman vortex street due to the natural convection. *Flow Visualization III*, pp. 348-352 (1985).

[9] K. Hatanaka, M. Kawahara, A numerical study of vortex shedding around a heated/cooled of a cylinder by the three-step Taylor-Gaylerkin method. *Int. J. Numer. Methods Fluids* **21**, pp. 857-867 (1995).

[10] R.A. Ahmad, Z.H. Qureshi, Laminar mixed convection from a uniform heat flux horizontal cylinder in a crossflow. *J. Thermophys. Heat Transfer* **6**, pp. 277-287 (1992).

[11] B.S.V. Patnaik, P.S.A. Narayana, K.N. Seetharamu, Numerical simulation of vortex shedding past a circular cylinder under the influence of buoyancy. *Int. J. Heat Mass Transfer* **42**, pp. 3495-3507 (1999).

[12] R.N. Kieft, C.C.M. Rindt, A.A.V. Steenhoven, The wake behaviour behind a heated horizontal cylinder. *Experiments in Thermal and Fluid Science* **19**, pp. 183-193 (1999).

[13] H. Hu, M. Kochesfahani, The wake behind a heated cylinder in forced and mixed convection regimes, *ASME Summer Heat Transfer Conference*, ASME, San Francisco, CA, (2005).

[14] B.V. Khyati, H. Hui, Z.J. Wang, Numerical investigation of effect of buoyancy on the wake instability of a heated cylinder in contra flow. *AIAA*, **0801**, pp. 1-19 (2007).

[15] A.A. Soares, J. Anacleto, L. Caramelo, J.M. Ferreira and R.P. Chhabra, Mixed convection from a circular cylinder to power law fluids. *Ind. Eng. Chem. Res.* **48**(17), pp. 8219–8231 (2009)

[16] A.T. Srinivas, R.P. Bharti, R.P. Chhabra, Mixed convection heat transfer from a cylinder in power-law fluids: effect of aiding buoyancy. *Ind. Eng. Chem. Res.* **48**(21), pp. 9735–9754 (2009)

[17] R. Nazar, N. Amin, I. Pop, Mixed convection boundary-layer flow from a horizontal circular cylinder with a constant surface heat flux. *Heat and Mass Transfer*, **40**, 219-227 (2004).

[18] M.M. Zdravkovich, Flow around circular cylinders: Fundamentals, **Vol. I**, Oxford *University Press: Oxford*, U. K., (1997)

[19] M.M. Zdravkovich, Flow around circular cylinders: Applications, Oxford *University Press: Oxford*, U. K., **Vol. II**, (2003)

[20] A.A. Soares, J.M. Ferreira, R.P. Chhabra, Flow and forced convection heat transfer in crossflow of non-Newtonian fluids over a circular cylinder. *Ind. Eng. Chem. Res*. **44**, 5815-5827 (2005).

[21] I. Imai, On the asymptotic behavior of viscous .uid .ow at a great distance from a cylindrical body, with special reference to Filon's paradox. *Proc. Roy. Soc*. A **208**, 487-516 (1951).

[22] R.P. Bharti, R.P. Chhabra, V. Eswaran, Numerical study of the steady forced convection heat transfer from an unconfined circular cylinder. *Heat Mass Transfer* **43**, 639–648 (2007).